Surfactant-Assisted Synthesis of NiO-ZnO and NiO-CuO Nanocomposites for Enhanced Photocatalytic Degradation of Methylene Blue Under UV Light Irradiation

Hulugirgesh Degefu Weldekirstos[1]*, Birtukan Habtewold[2] and Daniel Manaye Kabtamu[1]

[1]Department of Chemistry, College of Natural and Computational Science, Debre Brehan University, Debre Berhan, Ethiopia, [2]Department of Physics, College of Natural and Computational Science, Debre Brehan University, Debre Berhan, Ethiopia

The photocatalytic process over semiconducting oxide surfaces has attracted worldwide attention as a potentially efficient, environmentally friendly, and low-cost method for wastewater treatment. This study presents a straightforward, inexpensive, and rapid route for the synthesis of nickel oxide (NiO) and its composites with zinc oxide (NiO/ZnO) and copper oxide (NiO/CuO) nanoparticles through the chemical precipitation method using capping agent-hexadecyltrimethylammonium bromide (CTAB) for photocatalytic degradation of the methylene blue dye. The structure, morphology, and elemental constituents were characterized by X-ray diffraction, scanning electron microscopy, and energy-dispersive X-ray spectroscopy. The energy band gap of pure NiO, NiO-ZnO, and NiO-CuO composites was evaluated using the Tauc plot from absorption spectra and resulted as 3.00, 2.90, and 3.25 eV, respectively. The optimum parameters for all photocatalysts were the following: pH 8, irradiation time 175 min, catalyst amount 75 mg, and dye concentration 7 mg/L. At these optimum parameters, the degradation efficiency of the prepared photocatalysts toward the MB dye achieved was 89.8% for NiO, 97% for NiO/ZnO, and 94.2% for NiO/CuO. The highest activity of the p-type/n-type (NiO/ZnO) nanocomposite for MB degradation is possibly due to electron–hole pair recombination inhibition by charge transfer processes. Therefore, semiconducting composite-based nanocatalysts such as NiO/ZnO with high photocatalytic activity are promising for future industrial applications to remove undesirable organic pollutants from the environment.

Keywords: metal oxides, surfactant, nanocomposites, photocatalysis, wastewater treatment, methylene blue dye

1 INTRODUCTION

One of the main problems for the world community is water pollution. It causes damage to the environment, including climate and living things (Manisalidis et al., 2020). The fate of environmental pollutants that have been released from textile sewage and other industrial processes, such as methylene blue (MB) dye, is one of the most critical concerns that need immediate action and

GRAPHICAL ABSRACT |
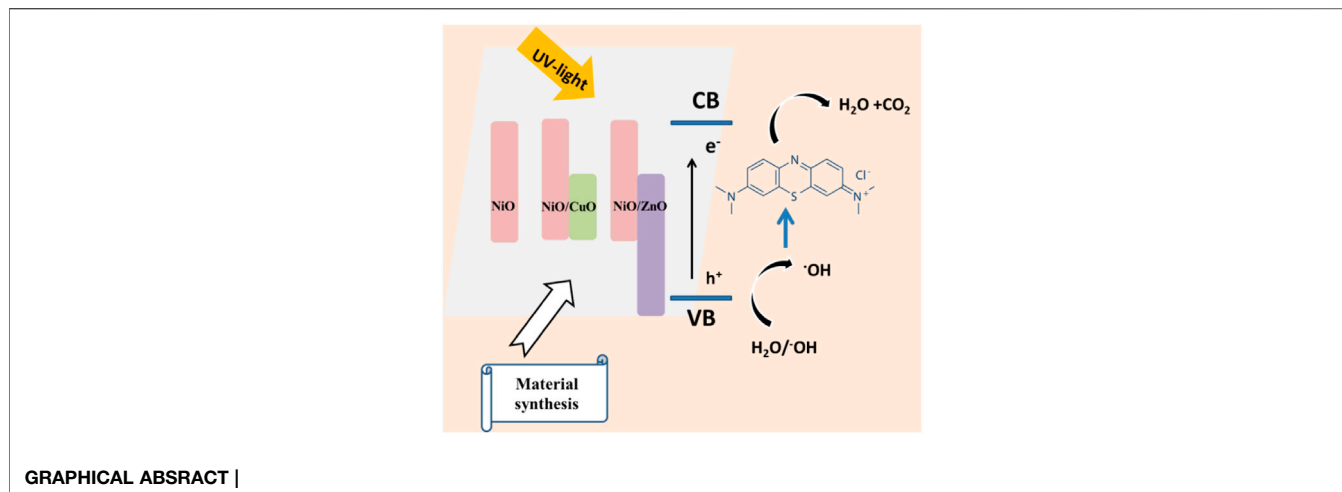
attention. Increasing population and human needs have resulted in the creation of numerous industries and factories, which has consequently increased the usage of water and raised the inevitable generation of wastewater. Textile industries have also been generating wastewater because of various consumable dyes (Pathak et al., 2020).

A large number of treatment processes have been employed in various industrial wastewaters such as chemical, biological, food, pharmaceutical, pulp and paper, dye processing, and textile wastes (Kong et al., 2019; Ni et al., 2020). The traditional physical techniques such as adsorption on activated carbon, ultrafiltration, reverse osmosis, coagulation by chemical agents, and ion exchange on synthetic adsorbent resins have been used for the removal of dye pollutants (Kumar and Dutta, 2019; Mani et al., 2019).

In recent years, semiconductor photocatalysis has been emerging as a promising technology and attracted increasing attention in the field of wastewater treatment to obtain complete mineralization of the pollutants of environmental systems (Aydoghmish et al., 2019; Iervolino et al., 2020; Prasad et al., 2020; Gao et al., 2021; Zhang et al., 2021). Over the past decade, research exertion has been dedicated to manufacturing new, more efficient and photoactive semiconductor nanostructures to transform the pollutants into safe byproducts devoid of any toxic hazardous chemicals from the environment (Liang et al., 2019). In particular, there has been an incredible improvement over the past decade in the synthesis of semiconducting metal oxides and sulfide nanoparticles with good yield. Semiconductor metal oxides such as TiO_2, ZnO, ZnS, CuS, and NiO have widely been studied and utilized in photocatalysis (Akerdi and Bahrami, 2019).

Among these semiconductor metal oxides, nickel oxide is a *p*-type semiconductor with a stable, low-cost, broad band gap and is nontoxic. Likewise, it has excellent optical, electrical, and photocatalytic properties making it a promising material for applications in photocatalysis (Han et al., 2019). To improve the photocatalytic activity of nickel oxide, considerable efforts have been devoted toward the modification of NiO *via* doping with nonmetals and addition of transition metals and coupled with semiconductors (Ramasami et al., 2015; Sankar et al., 2016;

Joyal Mary et al., 2017; Khatri and Rana, 2019). The previous report has demonstrated that the combination of two or more semiconductors with appropriate band positions can improve photocatalytic performance by enhancement of charge separation efficiency and prolonged charge carrier lifetime. Thus, the coupling of different semiconductor oxides is considered one of the most effective strategies, leading to high photocatalytic degradation.

Recently, different types of metal oxide nanocomposites such as ZnO/Mg, CuO/ZnO, ZnO/NiO, and CeO_2/ZnO have been synthesized and showed efficient photocatalytic activities (Morasae Samadi et al., 2016; Adil Shafi et al., 2019). ZnMgAl LTH/ZnO/g-C_3N_4 nanohybrid, Sn-doped ZnO, and SnO_2/PANI nanocomposite are also newly reported metal oxide-based materials for the application of photocatalysis (Munawar et al., 2021; Rajaji et al., 2021; Selvinsimpson et al., 2021). Among these composite materials, NiO/ZnO hetero-structural nanomaterials have attracted steadily growing interest as a result of the interesting electronic structure of NiO, a p-type semiconductor (E_g = 3.5 eV) with a rock salt or cubic structure (Zhao et al., 2017; Ao et al., 2019). NiO possesses high hole mobility and a low lattice mismatch with ZnO, which can be employed in the fabrication of p–n heterojunctions with ZnO (Aydoghmish et al., 2019; Song et al., 2019; Ramgir et al., 2020). On the other side, Joyal Mary et al. prepared CuO/NiO (p-type/p-type) by the co-precipitation method in the presence of a capping agent and investigated the visible light-driven photocatalytic degradation of Congo red (Joyal Mary et al., 2017).

Nowadays, the introduction of surfactants in the preparation of metal oxides has attracted much attention as a feasible and valuable method to control the surface properties of the material, such as the morphological structure, specific surface area, and particle size causes the chemical reactivity improvement. The stability of nanoparticles and their small size scale are important factors that determine their potential application. The presence of a stabilizer confines the particle in the nanometer scale, and after complete growth, the stabilizer restricts the nanoparticles to get agglomerate and small size nanoparticles (Guerrero-Florez et al., 2019; Saelices et al., 2019).

To the best of our knowledge, the synthesis of these metal oxide composites using the surfactant CTAB has not been reported. In addition to this, the photocatalytic efficiency of p-type/n-type (NiO/ZnO) and p-type/p-type (NiO/CuO) together in consideration of band gap and charge transfer difference was not studied so far. Here, our concern is on the synthesis of these materials in the presence of CTAB and the photocatalytic performance comparison of NiO, NiO/ZnO, and NiO/CuO on the degradation of methylene blue (MB) dye.

2 EXPERIMENTAL SECTION

2.1 Characterization Methods

We have used the following characterization methods throughout this work. Powder X-Ray diffraction patterns were recorded when 2θ value was in the range of 10–90° using a Brüker D8 Advance diffractometer (Cu Ka, 40 kV, 40 mA). Morphology and elemental analysis of the prepared photocatalysts were carried out using a field-emission scanning electron microscope with a model (ULTRA PLUS, a member of Carl Zeiss) and energy-dispersive X-ray spectroscopy (EDS), respectively. The Brunauer–Emmett–Teller (BET) specific surface area measurements were carried out with a micrometrics ASAP 2020 surface area and porosity analyzer. UV-Visible absorption spectroscopy measurements for photocatalyst band gap investigation and dye degradation efficiency analysis were carried out using a UV–Vis absorption spectrophotometer (SP65).

2.2 Synthesis of NiO, NiO/ZnO, and NiO/CuO

NiO was prepared using the chemical precipitation method, as described previously with some modifications (Khatri and Rana, 2019; Weldekirstos et al., 2019). First, two separate solutions were prepared; solution 1: 2 g of $NiCl_2.6H_2O$ and 1.5 g of CTAB were dissolved in 50 ml deionized water, and solution 2: 1.68 g of sodium hydroxide (NaOH) was added to 50 ml of distilled water. Then, the second solution was added to solution one slowly and stirred for 1 h to get a homogeneous solution. The resultant light green solution was collected by centrifugation at 4000 rpm for 10 min and washed three times with deionized water to remove any impurities. The washed precipitates were dried in an oven at 85°C for seven h. After drying, the powder was subjected to calcination at 450°C in a muffle furnace for 3 h to yield black powder NiO NPs.

The NiO/ZnO nanocomposite was prepared, as described in previously reported work with some modifications (Hessien et al., 2020). To obtain the NiO/ZnO nanocomposites, 2.5 g of $NiCl_2.6H_2O$ and 2 g of Zn $(NO_3)_2.6H_2O$ in a 1.5:1 M ratio, respectively, were dissolved in 60 ml distilled water, and then, 1.5 g of CTAB was added. The aqueous solution was stirred using a magnetic stirrer for 10 min to get a homogeneous solution. Subsequently, 0.042 mol solution of NaOH solution was added dropwise to the mixed solution under continuous stirring for 1 h. Then, the precipitate was centrifuged to 4000 rpm for 10 min and washed with excess distilled water three times, and the washed precipitate was dried at 85°C for 7 h in the air oven. Then, the final
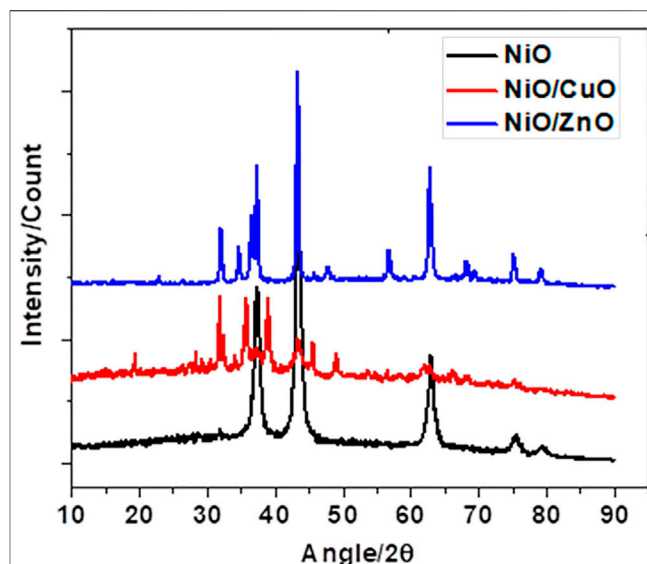
FIGURE 1 | XRD patterns for the NiO, NiO/CuO, and NiO/ZnO nanomaterials prepared with CTAB.

product was calcinated at 450°C for 3 h to get the NiO/ZnO nanocomposite.

NiO/CuO nanocomposite was synthesized following a similar procedure as NiO/ZnO nanocomposite by replacing Zn (NO_3) $6H_2O$ with copper (II) sulfate pentahydrate $(CuSO_4.5H_2O)$ for the abovementioned mechanism. In short, 2.5 g $NiCl_2.6H_2O$ and 2 g $CuSO_4.5H_2O$ in a 1.3:1 molar ratio, respectively, were dissolved in 60 ml of double distilled water, and then, 1.5 g of CTAB was added. The mixed solution was stirred for 10 min. Afterward, 0.042 mol solution of NaOH solution was added dropwise to this mixed solution under continuous stirring for 1 h. The resulting light blue precipitate was centrifuged at 4000 rpm for 10 min, washed with distilled water to remove any impurity, and then dried in an air oven at 85°C for 7 h. Finally, the NiO/CuO nanocomposite was obtained after calcination at 450°C for 3 h.

2.3 Photocatalytic Activity Test

The photocatalytic activity of the synthesized materials was evaluated as the degradation of a model pollutant, methylene blue, under UV light (generated by 8 W mercury lamp, 365 nm). The photocatalytic studies were performed to investigate NiO, NiO/ZnO, and NiO/CuO nanocatalyst performance for the degradation of MB dye. The experiments were carried out as follows. The stock solution (1000 mg/L) of MB was prepared using distilled water. The desired concentration of dye solutions was prepared by further dilution of the stock solution with distilled water. The photocatalytic performance of NiO, NiO/ZnO, and NiO/ CuO nanocatalyst was investigated at various pH (2–10) of solution, irradiation time (25–200 min, concentrations of MB (7–35 mg/L), and dose of photocatalyst (25–125 mg). The pH of the solution was adjusted by adding either 0.1 mol HCl or 0.1 mol NaOH.

Materials	Average crystallite size (nm)
NiO	7.32
NiO/ZnO	19.77
NiO/CuO	20.88

Materials	Surface area, BET (m²/g)
NiO/ZnO	41.05
NiO/CuO	19.33

The reaction suspensions were prepared by adding the photocatalyst (50 mg) to 100 ml of a 14 mg/L MB solution. After stirring in the dark for 30 min to obtain a good dispersion and ensuring an adsorption/desorption equilibrium, the suspension was exposed to UV light irradiation. Each time, the concentration of dye in the solutions was analyzed using a UV–Vis spectrophotometer by checking the absorbance at 664 nm during the degradation process. The percentage dye removal was calculated using the following equation:

$$Degradation\,(\%) = \frac{A_0 - A_t}{A_t} \times 100,$$

where A_o and A_t refer to the absorbance of the dye solution before and after the photocatalytic activity.

3 RESULTS AND DISCUSSION

3.1 Characterization of the Prepared Materials

3.1.1 Powder X-Ray Diffraction Study

Powder X-ray diffraction is the most useful technique for phase identification and structural parameters of the synthesized materials. The X-ray diffraction patterns of nanocomposites (NiO/ZnO and NiO/CuO) along with the individual phases of NiO are depicted in **Figure 1**. The XRD pattern of NiO in **Figure 1** showed that the synthesized material revealed sharpened peaks, indicating the crystallinity of NiO. The peaks positioned appearing at 2θ values of 37.06°, 43.20°, 62.75°, 75.48°, and 79.24° and each peak designated as (111), (200), (220), (311), and (222), respectively. These identified
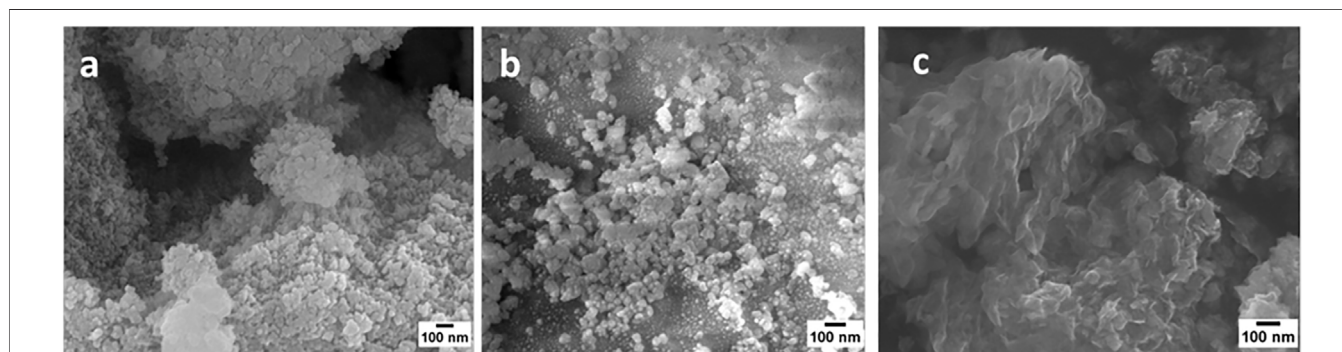
peaks were well indexed to face-centered cubic (FCC) of the NiO phase (JCPDS cared no. 00-047-1049). The XRD patterns of ZnO/NiO composite contain peaks at 31.2°, 33.7°, 35.6°, 46.7°, 55.8°, 67.3°, and 68.6° of ZnO and were well matched with the standard (JCPDS No. 76-0704) and in good agreement with the hexagonal phase. The XRD patterns of the NiO/ZnO nanocomposite exhibit peaks at 2θ values (100), (002), (101), (102), (110), (112), and (201) and are related to the hexagonal phase of ZnO crystal planes, respectively.
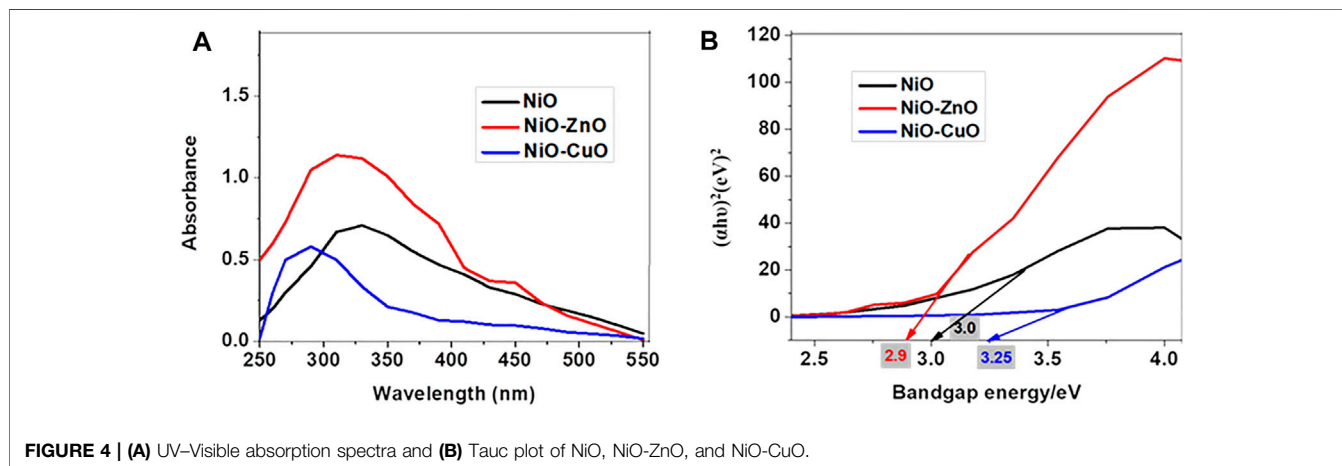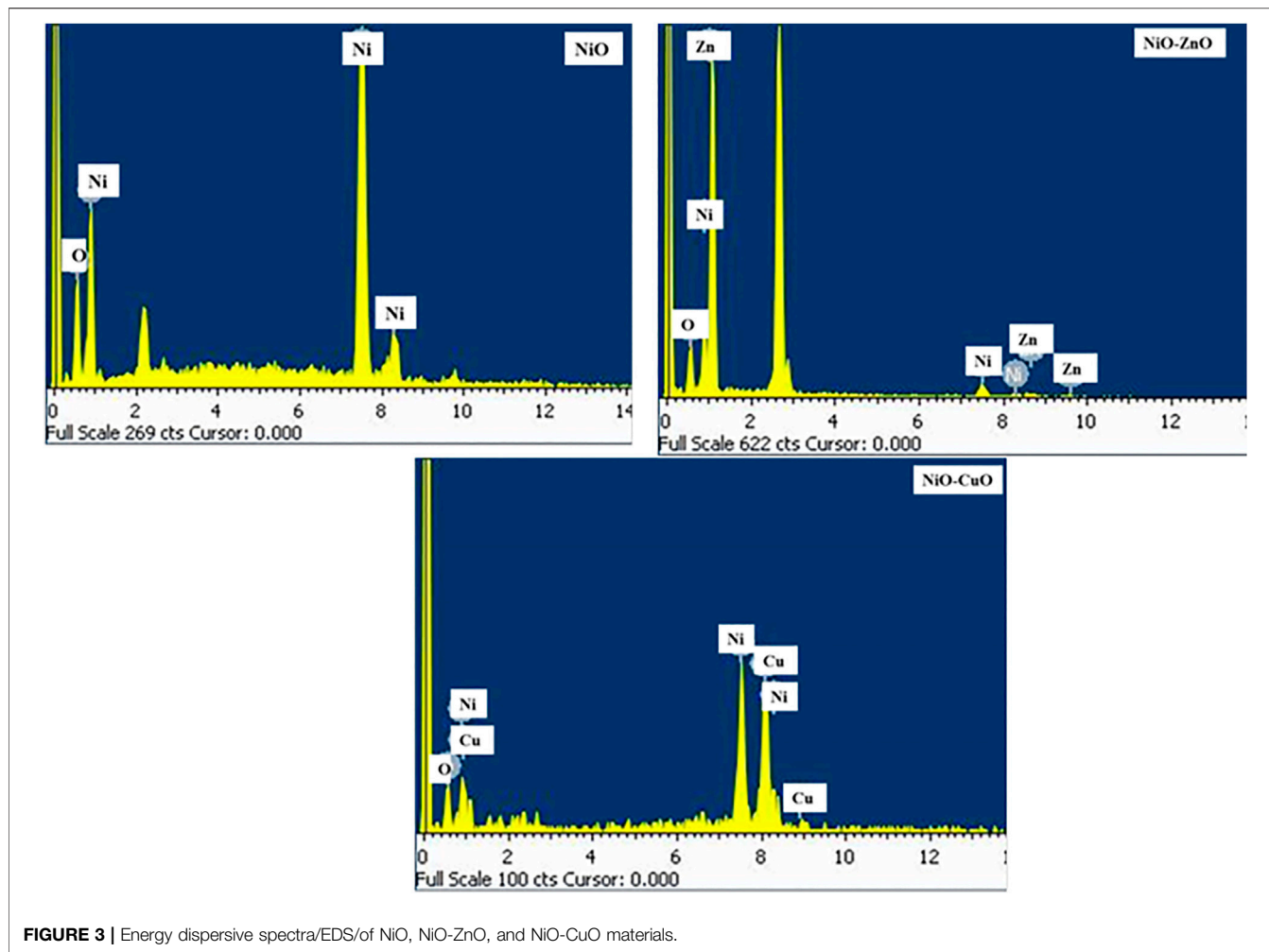
On the other hand, for NiO/CuO nanocomposite, the diffraction peaks located at 2θ values of 31.41°, 35.45°, 38.49°, 45.37°, 49.27°, 58.30°, 66.41°, and 68.16 indexed to the monoclinic phase of CuO crystal planes (110), (11-1), (111), (202), (020), (202), (31-1), and (211), respectively, which match with JCPDS no. 00-048-1548. Meanwhile, the intensity of the diffraction peaks is reduced with NiO/CuO composite, which breaks the crystallinity due to lattice distortion (Kumar et al., 2020).

The average crystallite sizes of NiO, NiO/ZnO, and NiO/CuO materials obtained from the Scherrer equation are presented in **Table 1**. The average crystallite size of these prepared materials was calculated by applying the Scherrer equation: $D = (K\lambda)/(\beta\cos\theta)$, where D is the average crystallite size, $\lambda = 1.54056$ Å is the wavelength of Cu kα, β is the full width at half-maximum (FWHM) intensity, θ is Bragg's diffraction angle, and K is a constant taken as to 0.94. The calculated value in the table is the averages of the crystallite size from the four peaks of each material are found to be 7.32 nm, 19.77 nm, and 20.88 nm NiO, NiO/ZnO, and NiO/CuO, respectively. From the result in **Table 1**, the average crystallite size of NiO is less than that of the composites of NiO/ZnO and ZnO/CuO, possibly due to the mixed oxide formation in the composites.

FIGURE 2 | SEM images of NiO **(A)**, NiO/ZnO **(B)**, and NiO/CuO **(C)** materials.

FIGURE 3 | Energy dispersive spectra/EDS/of NiO, NiO-ZnO, and NiO-CuO materials.

FIGURE 4 | (A) UV–Visible absorption spectra and **(B)** Tauc plot of NiO, NiO-ZnO, and NiO-CuO.

3.1.2 Morphology and Elemental Analysis

As well-known photocatalytic activity is highly related to the morphology, particle size, and surface area of nanomaterials (Jassbyand et al., 2012; Park et al., 2013), the morphology of these nanoparticles is studied by scanning electron microscopy.

Figure 2 presents the SEM images of the prepared NiO (a), NiO/ZnO (b), and NiO/CuO (c) materials. As shown in **Figure 2** of the NiO/CuO composite SEM image, the particles are revealed as relatively agglomerated, whereas the NiO/ZnO composite particles are shown in the dispersed mode. The dispersed surface structure
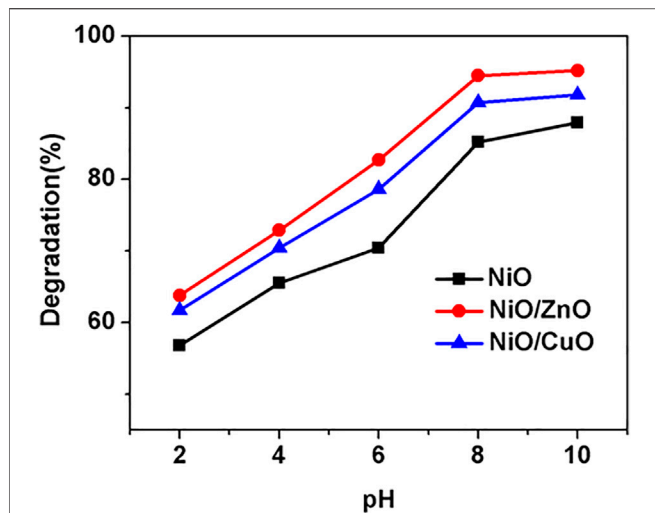
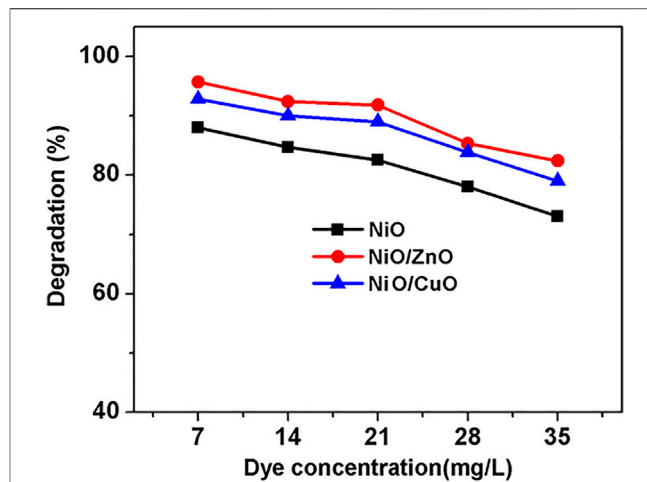**FIGURE 5 |** Effect of pH on degradation of methylene blue dye.

FIGURE 7 | Effect of MB concentration on photocatalytic degradation.
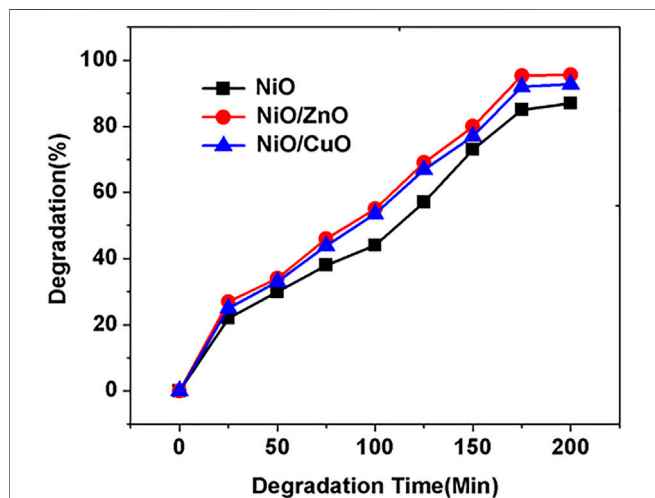

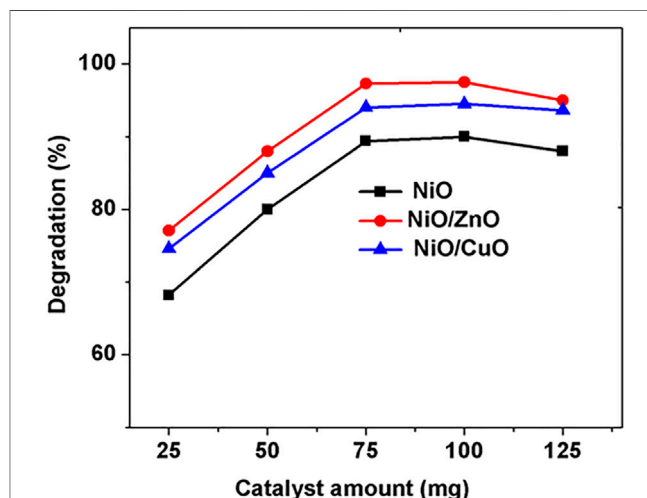**FIGURE 6 |** Effect of irradiation time on MB degradation.

FIGURE 8 | Effect of catalyst amount on MB degradation.

has higher surface area and positively influences the photocatalytic effectiveness of the material. For further information about the properties of these materials, the surface area measurement has been carried out for NiO/ZnO and NiO/CuO composites and presented in **Table 2**. The surface area (m^2/g) of NiO-ZnO and NiO-CuO composites attained was 41.05 and 19.33, respectively.

Energy-dispersive X-ray spectroscopy was investigated to identify the elements present in the prepared photocatalysts. **Figure 3** shows the EDS elemental mappings corresponding to all NiO, NiO/ZnO, and NiO/CuO samples. The presence of elements Ni and O in NiO; Ni, Zn, and O in NiO/ZnO; and Ni, Cu, and O in NiO/CuO are confirmed without any other impurity species.

3.1.3 Optical Properties
The optical properties of NiO, NiO-ZnO, and NiO-CuO materials were studied by UV-VIS absorption spectroscopy.

The UV–Visible absorption spectra of prepared samples NiO, NiO-ZnO, and NiO-CuO are shown in **Figure 4A**. The UV–Vis absorbance of the NiO-ZnO composite obtained was higher than the NiO-CuO composite and pure NiO, which implied that NiO-ZnO have relatively better light-harvesting efficiency. From the result, strong absorption peaks appeared at wavelengths of 330, 310, and 290 nm for pure NiO, NiO/ZnO, and NiO/CuO samples, respectively. The NiO-ZnO and NiO-CuO composites achieved blue shifted absorption compared to pure NiO. The band gap energy of the prepared samples was evaluated using the Tauc plot and is presented in **Figure 4B**. As shown in **Figure 4B**, the energy band gaps of pure NiO, NiO-ZnO, and NiO-CuO composites are found to be 3.0, 2.9, and 3.25 eV, respectively.

3.2 Photocatalytic Activity Study
To estimate the photocatalytic performance of the synthesized NiO, NiO/ZnO, and NiO/CuO samples, a photocatalytic

FIGURE 9 | Effect of the catalyst type on the degradation of MB dye.
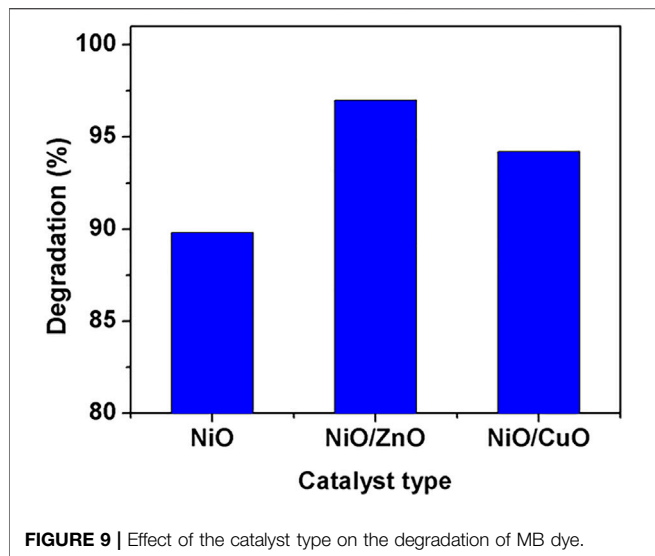
degradation experiment was carried out for methylene blue (MB) dye. The photocatalytic performance of NiO, NiO/ZnO, and NiO/CuO materials was investigated at various conditions: pH, irradiation time, concentrations of MB, and dose of the photocatalyst. Parameter optimization experiments have been carried out for pH, dye concentration, catalyst amount, and irradiation time to determine the most effective condition.

3.2.1 Effect of pH

One of the important parameters in photocatalytic reactions is the pH of the solution. It has a significant effect on the surface charge of the photocatalyst (Reza et al., 2017). The effect of the solution pH on the rate of photocatalytic degradation in the presence of NiO, NiO/ZnO, and NiO/CuO materials was investigated within different pH ranges from 2 to 10 (2, 4, 6,
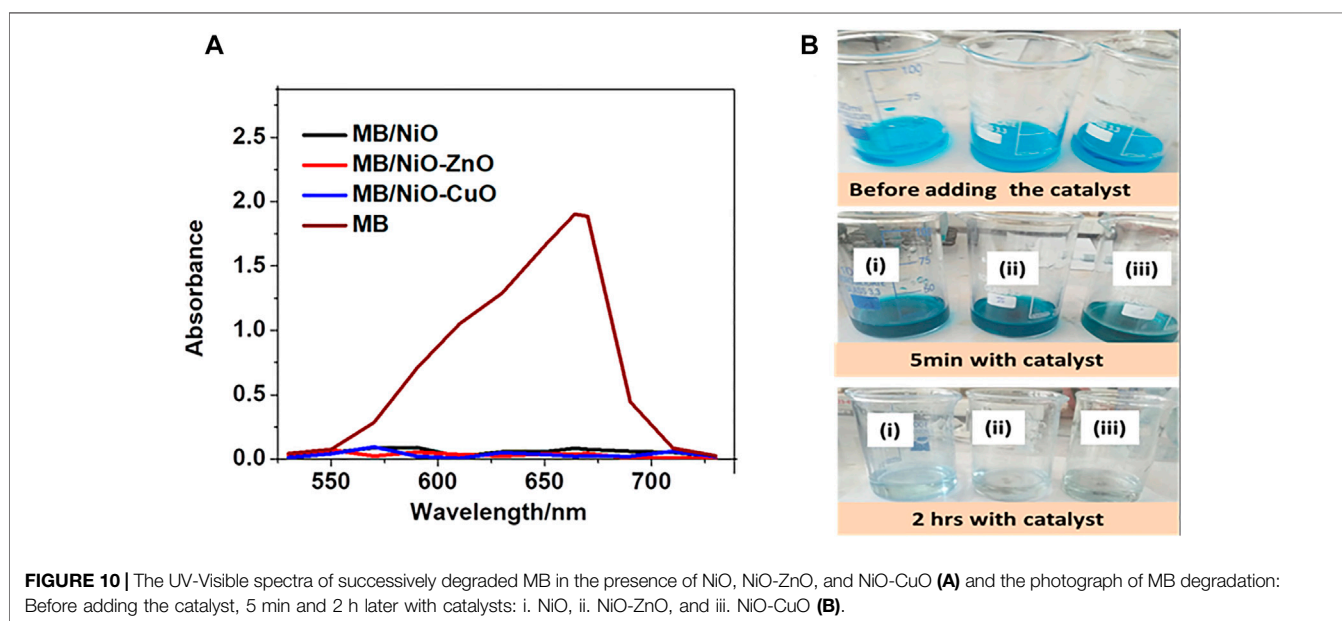
8, and 10), as shown in **Figure 5**. From the experimental result, an increase in the rate of photocatalytic degradation of MB was observed with an increase in pH from 2 to 8. Above pH 8, the dye degradation process becomes constant. In acidic solution (pH < 6), the photodegradation of the dye is retarded by the high concentration of protons, resulting in lower degradation efficiency. Basic pH electrostatic interaction between catalyst surfaces and MB cation leads to strong adsorption with a correspondingly high rate of degradation. The obtained result has a good agreement with the explanation given before (Rys and Zollinger, 1972). Based on the result, the optimum pH was found to be eight, for which the percentages of dye removal were found to be 85.2%, 94.5%, and 90.7% for NiO, NiO/ZnO, and NiO/CuO catalyst, respectively.

3.2.2 Effect of Irradiation Time

Irradiation time is another parameter that affects the photocatalytic efficiency for the removal of MB dye by NiO, NiO/ZnO, and NiO/CuO nanocatalysts. The experiment was investigated at the optimized condition of pH 8, and the irradiation time was varied from 25 to 200 min, keeping other experimental conditions constant. **Figure 6** shows the obtained results of degradation efficiency versus irradiation time. The degradation efficiency of the prepared photocatalysts for MB grew with the irradiation time up to 175 min, and after that, the value remained constant. The optimum irradiation time was found to be 175 min for all samples with a dye removal efficiency of 85, 93, and 90% for NiO, NiO/ZnO, and NiO/CuO catalysts, respectively.

3.2.3 Effect of Dye Concentration

To determine the impact of dye concentration on the degradation efficiency of the synthesized photocatalyst, the experiment was conducted at optimized pH 8 and irradiation time 175 min by changing the MB concentration from 7 to 35 mg/L (7, 14, 21, 28, and 35). The obtained results of MB degradation efficiency are

FIGURE 10 | The UV-Visible spectra of successively degraded MB in the presence of NiO, NiO-ZnO, and NiO-CuO **(A)** and the photograph of MB degradation: Before adding the catalyst, 5 min and 2 h later with catalysts: i. NiO, ii. NiO-ZnO, and iii. NiO-CuO **(B)**.

TABLE 3 | Comparison of photocatalytic performance of materials toward the degradation of methylene blue.

Composite materials used as photocatalyst	Degradation efficiency (%)	Light source	References
PANi—NiO	76	visible light	Vidya and Balamurugan (2019)
CuO–MgO–ZnO	88.5	sunlight illumination	Munawar et al. (2021)
NiO–ZnO–Ag	94	UV–visible	Aydoghmish et al. (2019)
NiO-ZnO and NiO-CuO	97 and 94	UV lamp	This work

illustrated in **Figure 7**. The experimental result presented in **Figure 7** clearly shows that the degradation efficiency of the synthesized photocatalyst is inversely proportional to the dye concentration. Even at the higher concentration of MB (35 mg/L), all three catalysts could achieve over 70% degradation. The degradation rate is dependent on the formation of radicals by the photocatalyst and the interaction of radicals with the dye molecules. When the dye concentration is high, the production of hydroxyl radicals ($\cdot$OH) at the surface of the photocatalyst is reduced since the photocatalyst active locations are being protected *via* the dye ions. Furthermore, throughout the high concentrations of dyes, a significant value of ultraviolet radiation could be absorbed by dye molecules and reduce the amount of radiation (Han et al., 2019). Thus, the removal of MB was found to be better at low concentration, i.e., at 7 mg/L for all catalysts with a removal efficiency of 88, 95.7, and 92.3% for NiO, NiO/ZnO, and NiO/CuO, respectively. We took 7 mg/L concentration of MB for further investigation.

3.2.4 Effect of Photocatalyst Amount

The effect of photocatalyst amount for removal of MB dye was also studied by varying the amount of the photocatalyst from 25 to 125 mg with increments of 25 mg by keeping other experimental parameters at optimal condition (pH 8, 7 mg/L of MB dye solution, and 175 min irradiation time). The obtained result of the dye removal efficiency versus the amount of the photocatalyst is shown in **Figure 8**. As observed from the obtained result, the degradation efficiency of MB dye increases as the photocatalyst amount increases up to 75 mg, and at a higher photocatalyst amount, the degradation efficiency remains constant. By increasing the amount of the photocatalyst, the number of active sites that exist on the molecular levels will increase, resulting in enlarging the number of hydroxyl and superoxide radicals. However, increasing the concentration of photocatalyst beyond the optimum amount could result in the coagulation of catalyst nanoparticles; therefore, there would be less surface area and consequently less photon absorption, which would accordingly reduce the rate of photocatalyst degradation (Sharma et al., 2018). From the experimental result, the optimum photocatalyst amount was found to be 75 mg. The dye removal at the optimum dosage was 89.4, 96.2, and 93.8% for NiO, NiO/ZnO, and NiO/CuO, respectively.

Finally, the photocatalytic degradation experiment was performed at optimum conditions: pH 8, 7 mg/L MB solution, 75 mg catalyst amount, and 175 min irradiation time for the three photocatalysts (NiO/ZnO, NiO/CuO, and NiO). **Figure 9** shows the graphical representation for the degradation efficiency result corresponding to the three materials. From the result, the NiO/ZnO composite achieved the highest degradation efficiency toward MB dye. When the p-type NiO and n-type ZnO materials were excited by UV light, electrons in the valance band could be excited to the conduction band, with the simultaneous generation of the same number of holes in the valance band. Hence, a p-type semiconductor NiO can act as a sink for photogenerated holes, making charge separation more efficient and thus suppressing recombination processes. The NiO catalyst alone lacked this capability, giving rise to less degradation activity (Liu et al., 2020).

The UV-Visible spectra of successively degraded methylene blue with the synthesized photocatalysts (NiO, NiO-ZnO, and NiO-CuO) after 2 h and the absorbance of methylene blue as a reference are presented in **Figure 10A**. **Figure 10B** demonstrates the pictures of the changes of the solution 5 min and 2 h later with the prepared photocatalysts: NiO, NiO-ZnO, and NiO-CuO. The absorbance spectra showed that at 2 h, there was nearly zero absorption which means that the methylene blue was successfully removed.

3.3 Comparison With Previously Reported Works

The comparison of the obtained degradation efficiency of MB using synthesized photocatalysts with previously reported findings has been illustrated in **Table 3**. Our findings show that in particular, the p-type/n-type composite (NiO/ZnO) achieved the highest photodegradation efficiency for MB dye.

4 CONCLUSION

In summary, pure NiO nanoparticles, NiO/ZnO, and NiO/CuO nanocomposites have been successfully prepared using the chemical precipitation method in the presence of CTAB as a surfactant. The three nanocatalysts (NiO, NiO/ZnO, and NiO/CuO) were used for the photocatalytic removal of MB dye under UV light irradiation. The metal oxides synthesized by the aforementioned method possess a high degree of purity, as indicated by the XRD patterns. The morphology and elemental investigations were studied by SEM and EDS, respectively. The experimental results of MB dye photodegradation confirmed that these materials could perform as promising photocatalysts. The photocatalytic efficiency of the synthesized nanomaterials followed the order: NiO/ZnO > NiO/CuO > NiO. The results indicated that the NiO/ZnO nanocomposite exhibited excellent photocatalytic activity as compared to NiO/CuO and NiO toward the degradation of MB

dye under UV light irradiation, while in the case of NiO/CuO nanocomposite, there should have been high e^-/h^+ recombination on CuO because of its narrow band gap.

DATA AVAILABILITY STATEMENT

The original contributions presented in the study are included in the article/Supplementary Material, further inquiries can be directed to the corresponding author.

AUTHOR CONTRIBUTIONS

All authors listed have made a substantial, direct, and intellectual contribution to the work and approved it for publication.

ACKNOWLEDGMENTS

REFERENCES

Akerdi, A. G., and Bahrami, S. H. (2019). Application of Heterogeneous Nano-Semiconductors for Photocatalytic Advanced Oxidation of Organic Compounds: a Review. *J. Environ. Chem. Eng.* 7 (5), 103283. doi:10.1016/j.jece.2019.103283

Ao, D., Li, Z., Fu, Y., Tang, Y., Yan, S., and Zu, X. (2019). Heterostructured NiO/ZnO Nanorod Arrays with Significantly Enhanced H2S Sensing Performance. *Nanomaterials* 9 (6), 900. doi:10.3390/nano9060900

Aydoghmish, S. M., Hassanzadeh-Tabrizi, S. A., and Saffar-Teluri, A. (2019). Facile Synthesis and Investigation of NiO-ZnO-Ag Nanocomposites as Efficient Photocatalysts for Degradation of Methylene Blue Dye. *Ceramics Int.* 45 (12), 14934–14942. doi:10.1016/j.ceramint.2019.04.229

Gao, L., Liu, J., Long, H., Wang, P., and Yu, H. (2021). One-step Calcination Synthesis of WC-Mo2C Heterojunction Nanoparticles as Novel H2-Production Cocatalysts for Enhanced Photocatalytic Activity of TiO2. *Catal. Sci. Tech* 11, 7307–7315. doi:10.1039/D1CY01581H

Guerrero-Florez, V., Blach, D., and Martínez, F. (2019). Nonpolar Interface Composition in Cetyltrimethylammonium Bromide Reverse Micellar Environments to Control Size and Induce Anisotropy on Gold Nanoparticles. *ChemistrySelect* 4 (47), 13983–13991. doi:10.1002/slct.201903844

Han, C., Zhang, R., Ye, Y., Wang, L., Ma, Z., Su, F., et al. (2019). Chainmail Co-catalyst of NiO Shell-Encapsulated Ni for Improving Photocatalytic CO2 Reduction over G-C3n4. *J. Mater. Chem. A* 7 (16), 9726–9735. doi:10.1039/c9ta01061k

Hessien, M., Da'na, E., and Taha, A. (2020). Phytoextract Assisted Hydrothermal Synthesis of ZnO–NiO Nanocomposites Using Neem Leaves Extract. *Ceramics Int.* 47, 811–816. doi:10.1016/j.ceramint.2020.08.192

Iervolino, G., Zammit, V., and Rizzo, L. (2020). Limitations and Prospects for Wastewater Treatment by UV and Visible-Light-Active Heterogeneous Photocatalysis: a Critical Review. *Top. Curr. Chem. (Cham)* 378 (1), 7. doi:10.1007/s41061-019-0272-1

Jassby, D., Farner Budarz, J., and Wiesner, M. (2012). Impact of Aggregate Size and Structure on the Photocatalytic Properties of TiO2 and ZnO Nanoparticles. *Environ. Sci. Technol.* 46, 6934–6941. doi:10.1021/es202009h

Jiménez Saelices, C., Save, M., and Capron, I. (2019). Synthesis of Latex Stabilized by Unmodified Cellulose Nanocrystals: the Effect of Monomers on Particle Size. *Polym. Chem.* 10 (6), 727–737. doi:10.1039/c8py01575a

Joyal Mary, D. D., Baiju, V., Biju, R., and Raveendran, R. (2017). PHOTOCATALYTIC DEGRADATION OF AZO DYE CONGO RED USING COPPER OXIDE/NICKEL OXIDE NANOCOMPOSITE. *Int. Jornal Adv. Res. Sci. Eng.* 06, 3. doi:10.1007/s13738-019-01767-3

Khatri, A., and Rana, P. (2019). Visible Light Photocatalysis of Methylene Blue Using Cobalt Substituted Cubic NiO Nanoparticles. *Bull. Mater. Sci.* 42 (4), 141. doi:10.1007/s12034-019-1835-z

Kong, Z., Li, L., Xue, Y., Yang, M., and Li, Y.-Y. (2019). Challenges and Prospects for the Anaerobic Treatment of Chemical-Industrial Organic Wastewater: a Review. *J. Clean. Prod.* 231, 913–927. doi:10.1016/j.jclepro.2019.05.233

Kumar, A., Kumar, A., and Krishnan, V. (2020). Perovskite Oxide Based Materials for Energy and Environment-Oriented Photocatalysis. *ACS Catal.* 10, 10253–10315. doi:10.1021/acscatal.0c02947

Kumar, S., and Dutta, V. (2019). Constructed Wetland Microcosms as Sustainable Technology for Domestic Wastewater Treatment: an Overview. *Environ. Sci. Pollut. Res.* 26 (12), 11662–11673. doi:10.1007/s11356-019-04816-9

Liang, Z., Yan, C.-F., Rtimi, S., and Bandara, J. (2019). Piezoelectric Materials for Catalytic/photocatalytic Removal of Pollutants: Recent Advances and Outlook. *Appl. Catal. B: Environ.* 241, 256–269. doi:10.1016/j.apcatb.2018.09.028

Liu, G., Abukhadra, M. R., El-Sherbeeny, A. M., Mostafa, A. M., and Elmeligy, M. A. (2020). Insight into the Photocatalytic Properties of diatomite@Ni/NiO Composite for Effective Photo-Degradation of Malachite green Dye and Photo-Reduction of Cr (VI) under Visible Light. *J. Environ. Manag.* 254, 109799. doi:10.1016/j.jenvman.2019.109799

Mani, S., Chowdhary, P., and Bharagava, R. N. (2019). "Textile Wastewater Dyes: Toxicity Profile and Treatment Approaches," in *Emerging and Eco-Friendly Approaches for Waste Management* (Springer), 219–244. doi:10.1007/978-981-10-8669-4_11

Manisalidis, I., Stavropoulou, E., Stavropoulos, A., and Bezirtzoglou, E. (2020). Environmental and Health Impacts of Air Pollution: A Review. *Front. Public Health* 8, 14. doi:10.3389/fpubh.2020.00014

Munawar, T., Mukhtar, F., Yasmeen, S., Naveed-ur-Rehman, M., Nadeem, M. S., Riaz, M., et al. (2021). Sunlight-induced Photocatalytic Degradation of Various Dyes and Bacterial Inactivation Using CuO-MgO-ZnO Nanocomposite. *Environ. Sci. Pollut. Res. Int.* 28, 42243–42260. doi:10.1007/s11356-021-13572-8

Ni, X.-Y., Liu, H., Xin, L., Xu, Z.-B., Wang, Y.-H., Peng, L., et al. (2020). Disinfection Performance and Mechanism of the Carbon Fiber-Based Flow-Through Electrode System (FES) towards Gram-Negative and Gram-Positive Bacteria. *Electrochimica Acta* 341, 135993. doi:10.1016/j.electacta.2020.135993

Park, Y., Kim, W., Tachikawa, T., Majima, T., and Choi, W. (2013). Role of Interparticle Charge Transfers in Agglomerated Photocatalyst Nanoparticles: Demonstration in Aqueous Suspension of Dye-Sensitized TiO2. *J. Phys. Chem. Lett.* 4, 189–194. doi:10.1021/jz301881d

Pathak, A. K., Kothari, R., Tyagi, V., and Anand, S. (2020). Integrated Approach for Textile Industry Wastewater for Efficient Hydrogen Production and Treatment through Solar PV Electrolysis. *Int. J. Hydrogen Energ.* 45, 48. doi:10.1016/j.ijhydene.2020.03.079

Prasad, C. L., Q., Tang, H., Yuvaraja, G., Long, J., Rammohan, A., and Zyryanov, G. V. (2020). An Overview of Graphene Oxide Supported Semiconductors Based Photocatalysts: Properties, Synthesis and Photocatalytic Applications. *J. Mol. Liquids* 297, 111826. doi:10.1016/j.molliq.2019.111826

Rajaji, U., Eva Gnana Dhana Rani, S., Chen, S.-M., Rajakumar, K., Govindasamy, M., Alzahrani, F. M., et al. (2021). Synergistic Photocatalytic Activity of SnO2/PANI Nanocomposite for the Removal of Direct Blue 15 under UV Light Irradiation. *Ceramics Int.* 47 (20), 29225–29231. doi:10.1016/j.ceramint.2021.07.087

Ramasami, A. K., Reddy, M. V., and Balakrishna, G. R. (2015). Combustion Synthesis and Characterization of NiO Nanoparticles. *Mater. Sci. Semiconductor Process.* 40, 194–202. doi:10.1016/j.mssp.2015.06.017

Ramgir, N., Bhusari, R., Rawat, N. S., Patil, S. J., Debnath, A. K., Gadkari, S. C., et al. (2020). TiO2/ZnO Heterostructure Nanowire Based NO2 Sensor. *Mater. Sci. Semiconductor Process.* 106, 104770. doi:10.1016/j.mssp.2019.104770

Reza, K. M., Kurny, A., and Gulshan, F. (2017). Parameters Affecting the Photocatalytic Degradation of Dyes Using TiO2: a Review. *Appl. Water Sci.* 7 (4), 1569–1578. doi:10.1007/s13201-015-0367-y

Rys, P., and Zollinger, H. (1972). *Fundamentals of the Chemistry and Application of Dyes*. London; New York: Wiley-Interscience.

Samadi, M., Zirak, M., Naseri, A., KhorashadizadeMoshfegh, E., and Moshfegh, A. Z. (2016). Recent Progress on Doped ZnO Nanostructures for Visible-Light Photocatalysis. *Thin Solid Films* 605, 2–19. doi:10.1016/j.tsf.2015.12.064

Sankar, S., Sharma, S. K., An, N., Lee, H., Kim, D. Y., Im, Y. B., et al. (2016). Photocatalytic Properties of Mn-Doped NiO Spherical Nanoparticles Synthesized from Sol-Gel Method. *Optik* 127 (22), 10727–10734. doi:10.1016/j.ijleo.2016.08.126

Selvinsimpson, S., Gnanamozhi, P., Pandiyan, V., Govindasamy, M., Habila, M. A., AlMasoud, N., et al. (2021). Synergetic Effect of Sn Doped ZnO Nanoparticles Synthesized via Ultrasonication Technique and its Photocatalytic and Antibacterial Activity. *Environ. Res.* 197, 111115. doi:10.1016/j.envres.2021.111115

Shafi, A., Ahmad, N., Sultana, S., and Khan, S. M. Z. (2019). Ag2S-Sensitized NiO-ZnO Heterostructures with Enhanced Visible Light Photocatalytic Activity and Acetone Sensing Property. *ACS Omega* 4, 12905–12918. doi:10.1021/acsomega.9b01261

Sharma, S., Sharma, R., and Sharma, A. K. (2018). Photo-Catalytic and Kinetic Study of Zinc Oxide Catalyzed Degradation of Copper Stearate Surfactants for Sustainable Development of Environment. *Cee* 5 (3), 221–229. doi:10.2174/2212717805666180801143324

Song, Z., Chen, W., Zhang, H., Li, Y., Zeng, W., Tang, S., et al. (2019). Highly Sensitive and Selective Acetylene Sensors Based on P-N Heterojunction of NiO Nanoparticles on Flower-like ZnO Structures. *Ceramics Int.* 45 (16), 19635–19643. doi:10.1016/j.ceramint.2019.06.212

Vidya, J., and Balamurugan, P. (2019). Photocatalytic Degradation of Methylene Blue Using PANi—NiO Nanocomposite under Visible Light Irradiation. *Mater. Res. Express* 6 (9), 0950c0958. doi:10.1088/2053-1591/ab34a3

Weldekirstos, H. D., Kuo, M.-C., Li, S.-R., Su, W.-L., Desta, M. A., Wu, W.-T., et al. (2019). New 2,3-diphenylquinoxaline Containing Organic D-A-π-A Dyes with

Nickel Oxide Photocathode Prepared by Surfactant-Mediated Synthesis for High Performance P-type Dye-Sensitized Solar Cells. *Dyes Pigm.* 163, 761–774. doi:10.1016/j.dyepig.2018.12.042

Zhang, K., Lu, G., Chu, F., and Huang, X. (2021). Au/TiO2 Nanobelts: thermal Enhancement vs. Plasmon Enhancement for Visible-Light-Driven Photocatalytic Selective Oxidation of Amines into Imines. *Catal. Sci. Tech* 11, 7060–7071. doi:10.1039/D1CY01333E

Zhao, Y., Liu, L., Cui, T., Tong, G., and Wu, W. (2017). Enhanced Photocatalytic Properties of ZnO/reduced Graphene Oxide Sheets (rGO) Composites with Controllable Morphology and Composition. *Appl. Surf. Sci.* 412, 58–68. doi:10.1016/j.apsusc.2017.03.207